2024 IEEE International Conference on Robotics and Automation (ICRA 2024)
May 13-17, 2024. Yokohama, Japan

Design of Highly Repeatable and Multi-Functional Grippers for Precision Handling with Articulated Robots

Philip Gümbel, Klaus Dröder

Abstract— **This paper presents a novel approach to designing, a low-cost gripper that is highly repeatable and functionally integrated. The gripper is optimized to compensate for gripping errors with particular consideration to potential challenges of articulated robots. The primary design goal is to achieve maximum repeatability during the gripping and releasing stages of a pick-and-place process for a chip-like silicon die. The design is centered around a custom printed circuit board integrates functionality for vision-based error compensation, vacuum level monitoring, part contact detection, and detection of abnormal vibrations. We detail our design requirements and specific design choices for the mechanical and electronic design and provide qualitative and quantitative experimental validation of the achieved repeatability and the integrated functions.**

I. Introduction

The continuously increasing demand for low-cost, high-precision assembly processes is being driven by technological advances, miniaturization, stringent quality standards, and specialized applications, such as autonomous driving. Although articulated robots (AR) are highly flexible and cost-effective, they are not traditionally used in these applications due to their low repeatability and even lower accuracy [1, 2] compared to purpose-built precision kinematics.

To address these fundamental challenges for serial kinematics of rotary joints, publications such as [3] and [4] develop empirical models to predict and optimize positioning performance. Publications such as [5] or [6] utilize similar model based approaches to further plan or optimizes handling processes.

In high-precision assembly processes with tolerances below 10 µm, secondary influences affecting handling repeatability are relevant, especially errors introduced during the grasping and release phases. The contact state between the grasped part and gripper is a major contributor to uncertainties. Grippers constructed from compliant materials, such as most commercial vacuum grippers, can cause positional errors of the grasped part due to gripper deformations. In the case of rigid grippers, suboptimal geometries can result in overly constrained contact states. For example, attempting to grip a deformed, scratched or dirty planar part with a planar vacuum gripper can result in an unstable contact resulting in the part tilting or shifting during the handling process. For mechanically insensitive parts, typically self-centering or self-aligning features are utilized [7, 8]. These are based on mechanical contact between the gripper and a specific feature of the part such as edges or corners.

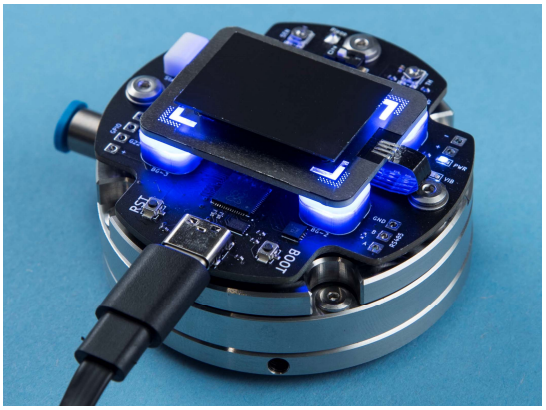

Figure 1. Developed gripper and handled silicon die.

If the part is initially gasped with a positional error, the clamping forces interacting with the centering features cause the part to shift into its reference pose. Aside from increased mechanical stress to the part, phenomena such as friction pose additional challenges to this approach.

For precise manipulation of mechanically delicate components, conventionally sensor-guided methods or specialized self-centering techniques such as leveraging capillary effects [9] and electrostatic forces [10], are employed. Sensor guided methods utilize sensors to measure the location of components prior to placement and can be employed in different stages of the handling process. Ideally, these measurements occur in close proximity to the placement phase to minimize gripping errors. Although feasible, actively compensating for part misalignment during placement via a feedback loop poses challenges arising from effects such as backlash or friction, particularly when operating at micrometer scale [11]. Consequently, active approaches often necessitate additional fine manipulation stages to address inaccuracies [12, 13].

In addition to errors introduced during gripping, the release stage results in further uncertainties. Particularly creating a defined contact of the part and its goal geometry is challenging when carried out without sensor guidance. Use of stiff part-gripper-interfaces can cause large contact forces in case of positional overshoot. While making contact between the part and its place location, not only the robots positional repeatability, but also its path tracking affect accurate positioning of the part. Thus, effects such as externally coupled oscillations, that are practically irrelevant during the robots transitional motion from pick to place pose [14], gain significant relevance, especially as AR are highly susceptible

P. Gümbel is with the Institute of Machine Tools and Production Technology, TU Braunschweig, 38106 Braunschweig Germany; Tel: +49-0531-391-7683; E-mail: p.guembel@tu-braunschweig.de.

Klaus Dröder is with the Institute of Machine Tools and Production Technology, TU Braunschweig, 38106 Braunschweig Germany

to vibrations due easy excitation at their comparatively low natural frequencies [15, 16]. In the worst case, positional errors as high as the oscillations amplitude may occur if present in the moment of making contact.

This work aims to address these errors in precision pick and place operations with ARs by designing a novel and functionally integrated gripper (shown in Fig. 1), enabling a reduction of AR-specific error sources.

II. Design Requirements

The gripper is to be designed for high precision pick and place of a 30 x 20 x 0.5 mm silicon die using a YASKAWA GP4 AR. The primary design goal is maximizing the pick and place repeatability, particularly regarding the previously discussed challanges of ARs in precision handling. The secondary goal is to maintain low cost to exploit the benefit of the comparatively low cost of ARs.

The selected operating principle is vacuum gripping. Mechanical grippers are considered unsuitable, due to the high risc of damaging the fragile edges and corners of the silicon die. More exotic actuation principles, such as electrostatic gripping, are avoided due to their high development and integration costs. To reduce the impact of varying die poses due to gripper deformations, a stiff interface between gripper and die is required. To further reduce impact of varying vacuum levels, a sensor for monitoring vacuum levels has to be integrated. The gripper additionally has to incorporate features to enable sensor-guidance to compensate for grasping errors. These include a background light to facilitate recognition of the die in transillumination and a reference feature on the gripper to enable relative measurements between gripper and die. To enable highly sensitivite gripping and placement of the fragile silicon die, the gripper also needs to integrate a contact or force sensor. To address the ARs sensitivity to vibrations, the gripper furthermore needs to integrate sensors for detection of abnormal vibrations. Finally, a RS485 interface is required for communication with a central process controller.

III. Mechanical Design

To bear the planar silicon die as repeatable as possible, the grippers geometry in contact with the die (die-gripper-interface) is designed to establish a tri-point contact. This reduces the influence of both, gripper and die deformations in comparison to conventional planar suction pads. Considering the potential for significant stress concentrations from gripping forces with an ideal tri-point contact, the interface employs three pillars to evenly distribute these forces. For increased design versatility while maintaining affordability, the die-gripper-interface is fabricated using 3D printing technology (MSLA). Instead of a deformable seal between the contact points for vacuum integrity, our novel approach allows a continuous leakage stream of air, reducing the risk of damage to the die from contaminating particles imbedded into the seal and leveraging the leakage for a self-cleaning effect by capturing contaminants in filters. The dimensioning of the die-gripper-interface was optimized through computational fluid dynamics (CFD) modeling with ANSYS Fluent, ensuring an effective management of airflow and pressure. Fig. 2 shows the simplified setup used for this simulation.

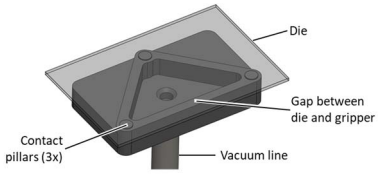

Figure 2. Simplified setup of die-gripper-interface with three contact pads and 30 cm vacuum line (not shown fully here) for CFD analysis.

The boundary conditions were defined as constant atmospheric pressure in the surrounding of the die and as pressure dependant mass flow at the end of a 30 cm vacuum line with 2 mm inner diameter. The mass flow characteristics were derived from the datasheet specifications of an SMC ZH07BS venturi pump. Targeting a maximum gripping force of 1 N, a suitable height of the contact pillars of 0.15 mm was chosen. This substantially exceeds the gravitational force (~0.0072 N) acting on the die and thereby affording considerable safety margins or the option to modulate the venturi pump's throughput to reduce air consumption. Fig. 3 shows the resulting air velocities as streamlines in (A) and the resulting pressure distribution at the die surface in (B). The average differential pressure at the dies surface is 16 mbar. With a surface area of 600 mm² this yields an anticipated gripping force of 0.96 N. The significant air velocity in the interstitial gap of ~50 m/s is deemed adequate for the extraction of contaminant particles. In operation, the gripper is actuated before making contact with the die, ensuring airflow over the contact pads, removing particulates on them. To enhance the repeatability of gripping forces, a pressure sensor is incorporated directly into the gripper cavity. This deviates from the traditional practice of positioning inline sensors upstream in the vacuum supply line, usually close to the vacuum generator (due to space constraints). Our novel integration strategy addresses the compressibility of air that significantly dampens air pressure fluctuations with increasing distance to the sensor. The direct placement within the cavity thus ensures a more immediate and precise response to changes in pressure at the actual contact interface.

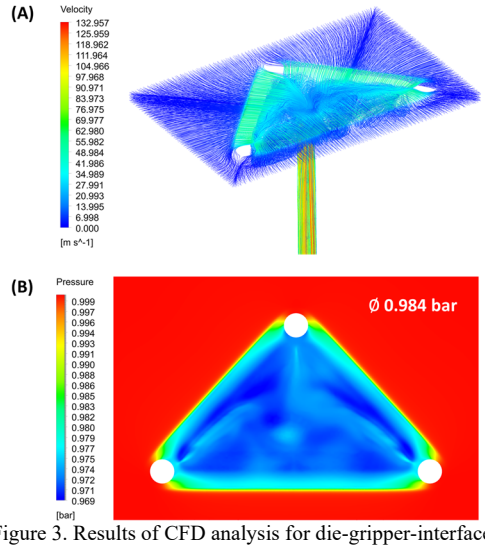

Figure 3. Results of CFD analysis for die-gripper-interface.
(A): Streamline velocities of leakage. **(B)**: Pressure at part surface.

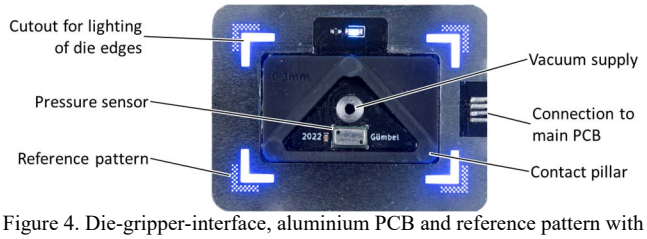

Figure 4. Die-gripper-interface, aluminium PCB and reference pattern with active background illumination.

To locate the sensor as closely as possible to the die, a surface mounted (SMD) sensor is chosen and mounted on an aluminium printed circuit board (PCB), which provides higher thermal stability compared to conventional FR4 substrate. The die-gripper-interface is bonded directly to the PCB using two-part epoxy adhesive. Additionally, a reference pattern mask for camera-based sensor guidance is attached to this PCB. Fig. 4 shows this assembly in detail. The stainless steel reference mask uses a pattern of 36 holes with 0.2 mm diameter. Circular features are selected, as they are robust to diameter variations, errors in circularity and the focus of the camera if combined with blob detection algorithms. L-shaped cut-outs allow for lighting the dies edges in transillumination. The patterns are designed to fit the field of view of 5 x 5 mm for the combination of a 2x magnification telecentric lens and a Sony IMX541 based camera. The mask itself was designed in ECAD software alongside the PCBs and ordered as a solder mask stencil, resulting in minimal additional cost.

The aluminium PCB is bonded to a hollow connecting stem supplying vacuum to the die-gripper-interface. This stem is attached to a drilled piezo disc, which is clamped by the upper and lower main body of the gripper. This arrangement results in contact forces between the die-gripper-interface and the die during picking or placing to be transferred directly to the piezo disc, causing it to deform and generate a voltage. This voltage is processed by the main PCB located on top of the upper body. The main PCB contains most of the electronic functions of the gripper (see Section IV). It integrates four miniaturized background lights to illuminate the reference pattern and the dies corners during image processing. The background lights use four LEDs emitting 445 nm light. Blue light was chosen due to its lower theoretical diffraction limit compared to red or green light and therefore higher potential resolution during image processing. The LEDs are covered by custom MSLA 3D printed diffusers with a non-uniform thickness (shown in Fig. 5), calculated from the LED directivity to provide a constant illumination of the background. Neither the main PCB, nor the diffusors are in direct contact with the aluminium PCB to minimize possible thermal impacts. The lower body itself is attached to the robot interface which uses four set screws for fine adjustment the planar translation and rotation of the gripper relative to the robots tool center point (TCP). Fig. 6 shows an explosion view of the gripper's assembly and the die as a reference.


Figure 5. Diffusor profile optimized for constant illumination.

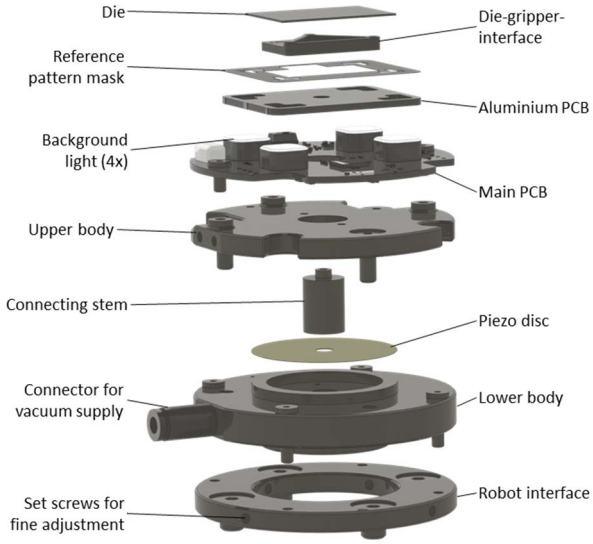

Figure 6. Explosion view of the gripper assembly and die.

IV. Electronic Design

The electronic design is centered around the main PCB (see Fig. 7) and designed using KiCad At the center of the PCB is a RP2040 micro controller (MCU), which provides two 133 MHz ARM Cortex-M0+ cores. A dual-core MCU enables parallel reading of sensors and communication with an external process controller. Programming of the MCU is achieved with the Arduino-pico core.

The design utilizes a four-layer PCB stack-up with dedicated internal ground and 3.3V power planes powered by a low dropout regulator. This specific stack-up allows easy power and ground routing with vias, reserving the front and back of the board for signal routing, at little extra cost over a double layer board.

For communication with the external process controller, the design integrates an RS485 interface IC connected to one of the RP2040's additional UARTs, allowing for robust communication over long distances in industrial settings. To drive the background LEDs, the board is equipped with two parallel Infineon BCR321U linear LED driver ICs per LED. These drivers drive the utilized Nichia NCSCE17AT LEDs close to their maximum forward current of 700 mA for flashing during image exposure or continuously with pulse width modulation dimming at up to 10 kHz. For precision vision applications, a short high intensity exposure is preferable to minimize motion blur caused by residual manipulator movement or vibrations during image acquisition. To meet the design requirement to detect vibrations during the handling process, the design uses an Inertial Measurement Unit (IMU, Bosch BMI160). The IMU combines a gyroscope with a sensitivity of up to 262.4 LSB/°/s in its lowest range (±125°/s) and a triaxial accelerometer with a sensitivity of 16384 LSB/g in its lowest range (±2 g). This particular IMU is a compromise between resolution, noise, features and cost. The IMU is connected via a dedicated i²c bus and positioned close to a mounting screw to minimize dampening and couple the gripper vibrations to it as directly as possible.

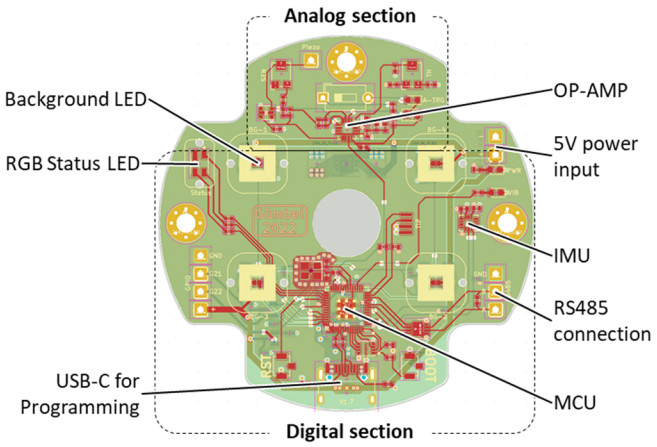

Figure 7. Layout of main PCB, divided into digital and analog sections.

Set to the accelerometer's maximum output data rate of 1600 Hz, the 3 dB cut-off frequency of 684 Hz (353 Hz for the Z-axis) results in sufficient temporal resolution, as the resonant frequencies of typical VAR structures are usually much lower [14, 17].

The remaining circuitry on the main PCB, located further away from the digital circuitry to improve signal integrity, realizes analogue signal processing of the piezo generated voltage for contact detection. It is built around a four channel LM324 operational amplifier (OP-AMP). The first channel of the OP-AMP is used as a buffer, providing a stable 1.65 V from a voltage divider to offset its second channel, which is set up as a differentiator. The voltage generated by the piezo element is fed into this differentiator. Using the third channel as a comparator, the voltage derivative is then compared to a reference voltage provided by a second voltage divider adjustable using a potentiometer. Adjusting the reference voltage allows the trigger point of the circuit to be fine-tuned. The output of the comparator is connected to an interrupt-controlled input of the RP2040. When the interrupt is triggered, the RP2040 responds via RS485 to the external process controller, stopping the robots motion. This analogue processing of the signal allows for a very fast response time and therefore a minimal overshoot, as well as minimal deflection of the piezo element and minimal forces between the gripper and die.

Lastly the aluminium PCB holding the pressure sensor board is connected to the main PCB via a flat-flex cable that provides power and a dedicated i²c bus for a Amsys MS5611 pressure sensor. This particular sensor was selected for its high pressure resolution (0.012 mbar), small footprint and good conversion time of down to 1 ms.

V. Experimental Evaluation

The gripper's functionality was evaluated in four sets of experiments. Firstly, the repeatability of the gripper was measured and compare to four commercially available vacuum grippers. Then the gripping force and functionality of the SMD pressure sensor was validated. Next, the capabilities of the integrated IMU of detecting vibrations were characterized. Lastly, the quality of the designed reference pattern for image processing was evaluated.

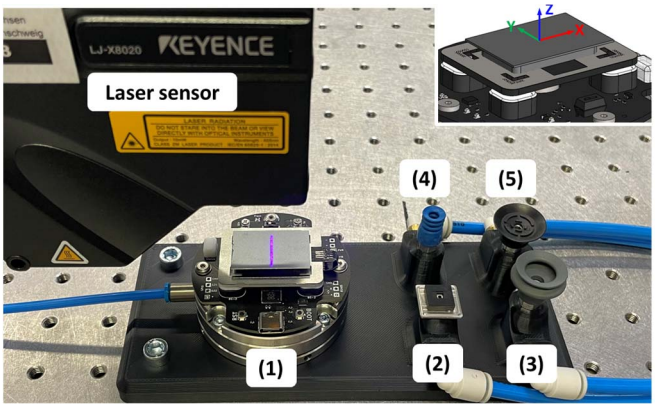

Figure 8. Experimental setup for RP investigation using a Keyence LJ-X8020 laser. **(1)**: Designed gripper. **(2)**: Hard rubber gripper for chips. **(3)**: Gripper with 1.5 bellows. **(4)**: Gripper with 2.5 bellows. **(5)**: Gripper with 0.5 bellows and supports for gripped part.

A. Evaluation of Repeatability and Comparison to Commercially Available Vacuum Grippers

The grippers' capability to repeatably fix the die in its locking feedoms (position in Z and orientation about X and Y) were characterized. Fig. 8 shows the experimental setup with a Keyence LJ-X8020 laser being mounted above the designed gripper (1) and four commercially available vacuum grippers (2-5) as references.

The experiments were carried out by positioning the sensor on top of each gripper successively and measuring the tilt (in X-axis) and Z-position of the die. In the first set of experiments the die was placed and the grippers repeatedly switched on and off for 10 cycles with 10 seconds on and off, to quantify the shift of the die as a result of actuation. Fig. 9 shows the resulting standard deviations of the die Z-position σ_Z and angle σ_A in red. The designed gripper outperformed the commercial grippers in both measures, showing no measurable angular deviations, compared to 0.017° for the next best gripper (3) and Z-position deviations of 0.516 µm compared to 2.486 µm for the next best gripper (2).

For a second set of experiments, the die was removed and repositioned with a vacuum pipette in between each repetition. Again, the gripper outperforms the commercial benchmarks with a standard deviation of the Z-position σ_Z of 3.773 µm compared to 3.917 µm for the next best (5) and angular standard deviation σ_A of 0.015° compared to 0.021° for the next best (4). During these experiments a significant hysteresis of both Z-position and angle was observed for the reference grippers (4) and (5). After switching on the grippers, the pose of the die drifted over several seconds. No such behavior was be observed for grippers (1), (2) and (3)

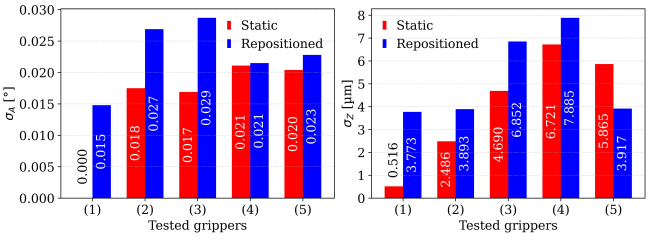

Figure 9. Standard deviation of die on gripper in Z-position σ_Z and angle σ_A.

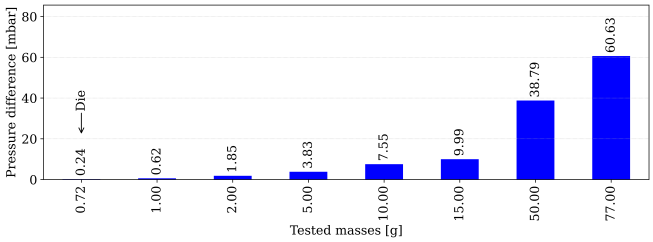

Figure 10. Required pressure difference for varying test masses. Means of five measurements. All standard deviations < 0.12 mbar.

B. *Differential Pressure and Part Mass*

To validate the expected gripping force of the CFD simulation and at the same time the functionality of the pressure sensor integrated into the gripper cavity, further experiments were performed. Using varying test masses held by the gripper as shown in Fig. 11 (A), firstly the grippers maximum capacity of 0.756 N (77g) was identified. While below the expected 0.96 N, likely as a result of the simplification of the gripper geometry, it still offers sufficient safety margins. Next, using 8 different test masses from 0.72 g (die) to 77.0 g, the pressure difference required to hold the test mass was determined , using the SMD pressure sensor (Fig. 10). As modelled, the pressure at the position of the sensor drops significantly due to the intended gaps leading to leaks. At the optimal operating point of the used venturi pump, a maximum difference of 60.03 mbar was observed. For practical applications, a differential pressure of around 10 mbar is chosen as a compromise between air consumption (~10 l/min at 2.5 bar), safety margin (~20x) and forces acting on the die. With an estimated ratio of pressure to gripper capacity of 1.5 g/mbar at this operating point, the pressure sensor with its resolution of 0.012 mbar is theoretically capable of resolving fluctuations in gripping strength of 0.018 g or 0.18 mN. Even with a noisy pressure signal (standard deviation measured as $\sigma_P = 0.064$ mbar) this allows for highly sensitive monitoring of the gripping force.

C. *Externally Coupled Oscillations and Impulses*

To investigate the ability of the IMU to detect externally coupled harmonic oscillations as well as impulses, another set of experiments was carried out. Using the experimental setup in Fig. 11, an eccentric oscillator (moment of inertia of 2254 g/mm²) was employed to stimulate the robot with a 100 s frequency sweep from 1 Hz to 100 Hz.

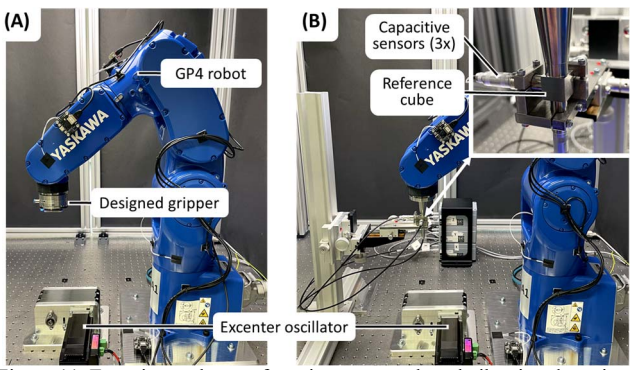

Figure 11. Experimental setup for gripper strength and vibration detection. **(A)**: Installed gripper. **(B):** Installed capacitive measuring system.

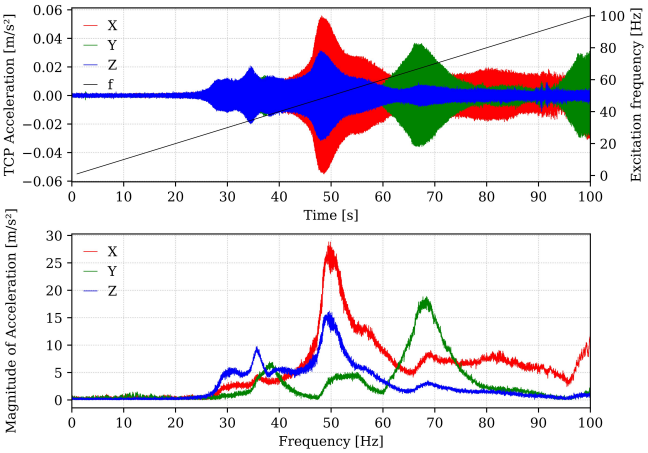

Figure 12. TCP oscillations in m/s² (IMU) resulting from external excitation with excenter oscillator. Z-axis is offset by the gravitational acceleration.

With the gripper mounted to the robot in Fig. 11 (A), the resulting accelerations measured by the IMU were recorded. The gripper was then changed to a reference cube and capacitive measuring system (Micro Epsilon capaNCDT600) to quantify the TCP position, as shown in Fig. 11 (B) and another sweep performed. In both setups, the measurements were recorded at 1 kHz sampling rate. Fig. 12 shows the resulting accelerations measured by the IMU as well as the FFT of the signals indicating initial resonances at around 35 Hz and significant resonances around 50 Hz and 70 Hz. Fig. 13 shows the corresponding signal of the TCP position and its FFT with resonances in similar regions. Slight differences are likely a result of differing masses on the TCP as well as mechanical properties of the capacitive measuring systems.

To further investigate the IMU's ability to detect sharp, discrete impulses applied to the system, a 0.00706 Ns impulse was applied by dropping a 5.01 g steel from a height of 10 cm, centered below the gripper. This was repeated in both setups of Fig. 11 (A) and (B). The resulting signals are shown in Fig. 14. The impact resulted in a minute TCP motion with a peak-to-peak amplitude of 0.9 µm. Although close to the temporal resolution limits of the IMU, the impact was detected with sufficient signal peak strength when compared to the baseline noise floor.

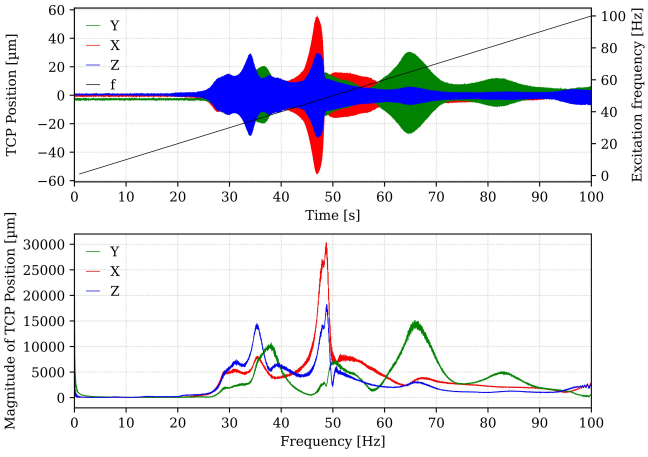

Figure 13. TCP oscillations in µm (capaNCDT) resulting from external excitation with excenter oscillator.

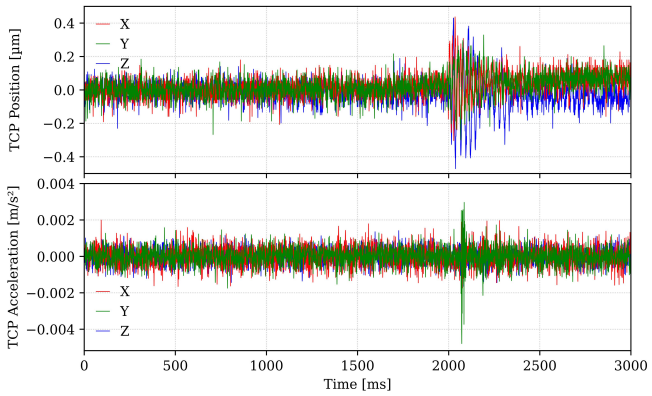

Figure 14. TCP oscillations in µm (capaNCDT) and m/s² (IMU) resulting from excitation with a 0.00706 Ns impulse.

D. *Image Quality of Part Edge and Gripper Pattern*

To evaluate the performance of the backlight and the chosen reference pattern, the setup shown in Fig. 15 was used, consisting of a camera (Sony IMC541 sensor chip with 2.74 µm pixel pitch) fitted with a 2x telecentric lens. This combination results in a theoretical resolution of 1.37 µm/pixel. Due to the very narrow depth of field, it is necessary to take individual images of the die edge and the reference pattern to calculate the part gripper offset based on them. In order to achieve this without the positional repeatability of the robot affecting the calculated offset, the camera was mounted on a high precision linear slide (linear repeatability of 0.5 µm) in line with the optical axis of the lens.

The captured images in Fig. 16 (B) show sharp transitions from the white background to the edge of the part pattern. When inspecting the holes edges (Fig. 16 (A)) closely, defects extending up to 6 µm towards the holes centers were visible. As the defects were evenly distributed around the holes diameter and over all 36 holes of the pattern and as the gripper position will be calculated by averaging the centers of gravity of all 36 holes, we consider the pattern quality to be adequate.

The pattern quality could be further optimized by using post-processing of the laser-cut sheet metal by electro-polishing [19, 20] or by advanced fabrication methods such as direct etching of the pattern [21].

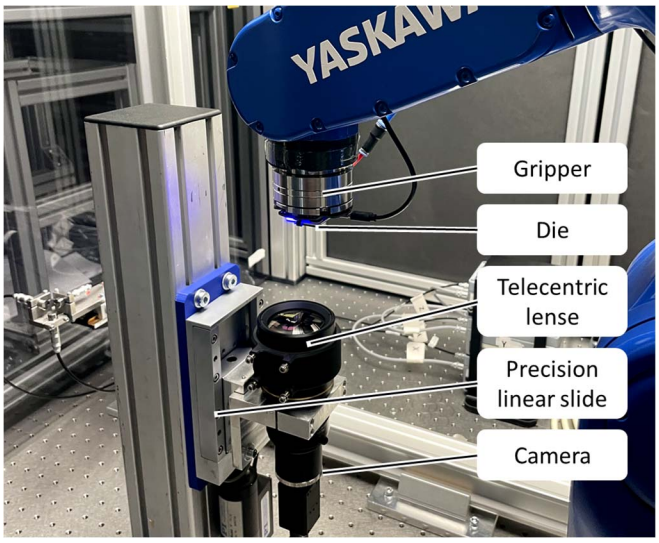

Figure 15. Camera setup for image processing.

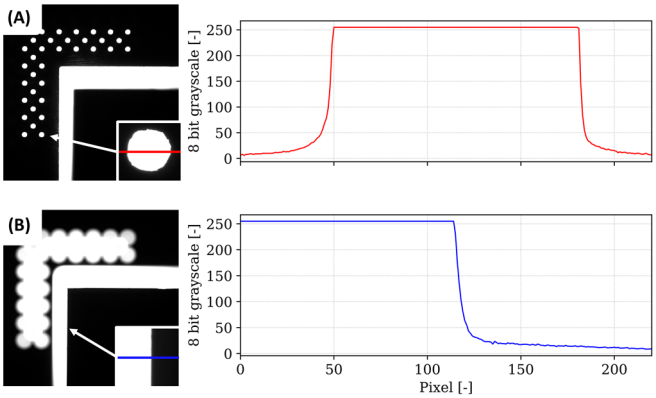

Figure 16. Greyscale transitions at pattern hole **(A)** and die edge **(B).**

VI. Discussion and Conclusion

We introduced a cost-effective, multifunctional gripper design for precise silicon die handling with ARs. The design incorporates sensors and capabilities aiming at minimizing gripping errors specific to ARs. The novel gripper design is intentionally leaky, offering a highly repeatable contact state between die and gripper and is capable of generating up to 0.756 N of gripping force. Its self-cleaning design further reduces possible impacts of particulates in the gripping process. Using custom PCBs, additional functionalities, such as in-gripper-monitoring of vacuum pressure, lighting for camera based sensor guidance, detections of vibrations and a high-speed analog contact sensor were implemented. Experimental evaluation demonstrate the superior repeatability compared to commercial grippers as well as the functionality of its additional features. With a material cost <100 € the potential of low cost SMD components and custom PCBs for achieving highly functionally integrated grippers was demonstrated. We excluded characterization on contact detection with the integrated piezo element, for a lack of sufficiently sensitive assessment methods. Preliminary findings indicate high sensitivity and suggest a potential parallel use of the piezo for vibration detection. Replacing the IMU with a high-bandwidth analog-to-digital converter could enhance sensitivity and temporal resolution.

Future implementations aiming to improve the IMU performance, could consider an array of parallel IMUs, allowing use of sensor fusion algorithms that reduce noise by the square root of the number of IMUs [18]. Furthermore, the use of IMUs to facilitate input shaping strategies [22, 23] that use self excitation to identify resonant frequencies and plan adjusted trajectories with minimal virbation could be ionvestigated. Finally Integration of SMD pressure sensors directly into the grippers cavity showed great potential and use in conventional, fully sealing vacuum grippers should be explored in the future.

Acknowledgment

This study was conducted independently and funded by the Institute of Machine Tools and Production Technology of TU Braunschweig.

REFERENCES

[1] J.-P. Merlet. *Parallel robots*. Vol. 128. Springer Science & Business Media, 2006.

[2] R. M. A. Nzue, J. F. Brethé, E. Vasselin and D. Lefebvre, "Comparison of serial and parallel robot repeatability based on different performance criteria." in *Mechanism and Machine Theory*, vol. 61, 2013, pp. 136-155.

[3] F. Azadivar, "The effect of joint position errors of industrial robots on their performance in manufacturing operations." in *IEEE Journal on Robotics and Automation*, vol. 3.2, 1987, pp. 109-114.

[4] Brethé, Jean-François, et al. "Modelling of repeatability phenomena using the stochastic ellipsoid approach." in *Robotica*, vol. 24.4, 2006, pp. 477-490.

[5] P. Gümbel, X. He and K. Dröder, "Precision optimized pose and trajectory planning for vertically articulated robot arms." in *Procedia CIRP*, vol. 106, 2022, pp. 185-190.

[6] J. Baumgärtner, P. Gönnheimer and J. Fleischer, "Optimal Robot Workpiece Placement for Maximized Repeatability." in *Advances in System-Integrated Intelligence*, 2022, pp: 252-261.

[7] M. Wagner, J. Morehouse and S. Melkote, "Prediction of part orientation error tolerance of a robotic gripper." in *Robotics and Computer-Integrated Manufacturing*, vol. 25.2, 2009, pp. 449-459.

[8] I. Simionescu, and C. Ionescu, "Optimum design of self centering grippers." in *Scientific Bulletin of University Politehnica of Bucharest, series D 1*, vol. 73, 2011, pp. 3-16.

[9] V. Sariola, V. Liimatainen, T. Tolonen, R. Udd, and Q. Zhou, (2011, May "Silicon capillary gripper with self-alignment capability." *IEEE International Conference on Robotics and Automation*, 2011, pp. 4098-4103.

[10] F. Biganzoli and G. Fantoni, "A self-centering electrostatic microgripper." in *Journal of Manufacturing Systems*, vol. 27.3, 2008, pp. 136-144.

[11] D. Dandash, J. F. Brethé, E. Vasselin, and D. Lefebvre, "Micrometre scale performances of industrial robot manipulators." *in International Journal of Advanced Robotic Systems*, vol. 9.4, 2012, pp. 159.

[12] C. Hegao, S. Lining, A. Hui, and Z. Tao, "A two-dimensional electrostrictive worktable for robot precise assembly." in *Proceedings of 1994 IEEE International Conference on Industrial Technology-ICIT'94*., 1994, pp. 560-564.

[13] Y. Ma, K. Du, D. Zhou, J. Zhang, X. Liu, and D. Xu, "Automatic precision robot assembly system with microscopic vision and force sensor." in *International Journal of Advanced Robotic Systems*, vol. 16.3, 2019.

[14] P. Gümbel and K. Dröder, "Systematic Investigation of Influences on the Repeatability of Vertically Articulated Robot Arms." in *Congress of the German Academic Association for Production Technology*, 2023, pp. 205-217.

[15] S. Li, S. Fan, J. Gu, X. Li, and Z. Huang, "Blind-Kriging based natural frequency modeling of industrial Robot." in *Precision Engineering*, vol. 74, 2022, pp. 126-139.

[16] K. Wu and B. Kuhlenkötter. "*Experimental analysis of the dynamic stiffness in industrial robots.*" in Applied Sciences, vol. 10.23, 2020, pp. 8332.

[17] Bisu, Claudiu, et al. "Dynamic behavior analysis for a six axis industrial machining robot." in *Advanced Materials Research*, vol. 423, 2012, pp. 65-76.

[18] I. Skog, J.-O. Nilsson, P. Händel and A. Nehorai, "Inertial sensor arrays, maximum likelihood, and cramér–rao bound." in *IEEE Transactions on Signal Processing*, vol. 64.16, 2016, pp. 4218-4227.

[19] M. Wickham, L. Zou, M. Dusek and C. Hunt, "Design guidelines for ultra fine pitch solder paste printing.", 2002.

[20] Lee, Yong-Won, Keun-Soo Kim, and Katsuaki Suganuma. "The behaviour of solder pastes in stencil printing with electropolishing process." in *Soldering & Surface Mount Technology*, vol. 25.3, 2013, pp. 164-174.

[21] E. K. Lo, N. N. Ekere, S. H. Mannan and I. Ismail, "The future of solder paste printing for SMT reflow soldering." in *Soldering & Surface Mount Technology*, vol. 5.1, 1993, pp. 22-32.

[22] N. C. Singer and W. P. Seering. "Preshaping command inputs to reduce system vibration.", in *Dynamic Systems Measurement and Control*, vol. 112, 1990, pp. 76-82.

[23] A. Kamel, F. Lange and G. Hirzinger. "An industrial-robots suited input shaping control scheme." in *Motion and Vibration Control*, 2009, pp. 177-188.